EARTHQUAKE ENGINEERING AND STRUCTURAL DYNAMICS, VOL. 26, 595–616 (1997)

TWO-DIMENSIONAL SCATTERING OF P, SV AND RAYLEIGH WAVES: PRELIMINARY RESULTS FOR THE VALLEY OF MEXICO

EDUARDO REINOSO,[1]* LUIS C. WROBEL[2] AND HENRY POWER[3]†

[1] *Instituto de Ingeniería, UNAM Ciudad Universitaria, Apartado Postal 70-472, México, D.F. 04510, MÉXICO*

[2] *Brunel University, Department of Mechanical Engineering, Uxbridge UB8 3PH, Middlesex, U.K.*

[3] *Wessex Institute of Technology, University of Portsmouth, Ashurst Lodge, Ashurst SO4 2AA, Southampton, U.K.*

SUMMARY

A direct boundary element method for calculating the two-dimensional scattering of seismic waves from irregular topographies and buried valleys due to incident P-, SV- and Rayleigh waves is employed to model a section of the Mexico City Valley. The method has been formulated with isoparametric quadratic boundary elements and contains, with respect to previous works in the field, some improvements that are briefly presented.

Because the Mexico City Valley is relatively flat and shallow and the contrast of S-waves between the clays and the basement rock is very high, it is believed that the one-dimensional theory is enough to explain the amplification patterns. Although this is true for most sites, results from recent accelerometric data suggest that two- and three-dimensional models are needed to explain the amplification behaviour at some places.

In this work, two accelerometric sites have been chosen: Site 84 to probe that the one-dimensional model works well for most sites, and Site TB, as an example of irregular response. The two-dimensional method presented here was used to model a section of the valley where site TB is located, showing that this method yields results closer to the observations than the one-dimensional approach. © 1997 by John Wiley & Sons, Ltd. Earthquake eng. struct. dyn. 26: 595–616, 1997.

(No. of Figures: 17. No. of Tables: 0. No. of Refs: 33.)

KEY WORDS: valley; Mexico City; scattering; seismic waves; accelerometric data; boundary element

INTRODUCTION

The extensive damage observed during recent earthquakes on human settlements located over alluvial valleys has encouraged studies of site amplification. For the last 25 years the seismic effects of buried valleys and topographic and subsurface irregularities have been extensively studied. Important theoretical and experimental results have been obtained but the identification of such effects on the observed records has not been satisfactorily found.

Although the amplification caused by infinite flat layers is well documented through the one-dimensional theory (1D), most valleys are of finite size where borders and geometry play an important role modifying the 1D response and generating surface waves. For such problems, two- (2D) and three-dimensional (3D) models of wave propagation are needed.

The easiest way to solve 2D scattering is considering SH-wave propagation. This is a scalar problem in which the Helmholtz equation is solved. For P-, SV- and Rayleigh waves, the problem is vectorial and the solution of the equations of elastodynamics is required. For simple geometries, analytical solutions for

* Correspondence to: E. Reinoso, UNAM, Instituto de Ingenieria, Ciudad Universitaria, Apartado Postal 70-472, Coyoacan 04510, Mexico D.F.

† On leave from Universidad Central de Venezuela, Caracas, Venezuela.

Contract grant sponsor: National Council for Science and Technology (CONACyT).
Contract grant sponsor: Government of Mexico City (Secretaría General de Obras y Servicios del Departamento del Distrito Federal).

CCC 0098–8847/97/060595–22$17·50

Received 16 January 1996
Revised 17 October 1996

P- and SV-waves have been obtained, but for more realistic configurations, numerical methods have to be used. The boundary element method is now very popular due to its efficiency to represent infinite domains and geometries. Other methods that have been applied are the Aki–Larner method, the finite difference method and the finite element method. The combination of finite and boundary elements is particularly convenient when dealing with inhomogeneous, anisotropic and non-linear problems. More recently, an increasing effort to model realistic configurations for 2D valleys can be found in the literature. Some of these works are: for Los Angeles Basin,[1,2] for the Ubaye valley in the French Alps[3] and for the Caracas Basin.[4]

Owing to the dynamic characteristics of the clay deposits upon which Mexico City rests, the valley is one of the best examples of amplification in alluvial basins. The complexity of the whole response of the valley requires reliable 1D, 2D and 3D models. Because of the size, shallowness, slow shear-wave velocity of the soil which fill the valley and the lack of accurate information of the strata and deep structure, detailed 3D modelling is still far from being realistic. However, important 1D and 2D results have been obtained that can explain some features of the valley amplification.

Since 1985, the accelerometric network of Mexico City has grown considerably and now provides useful strong motion data to study the amplification patterns of the valley. Since then, numerical models have been used in order to understand the seismic response of the valley. Most of these works compare, in some way, modelling results with observed data.[5–16] Bard *et al.*[5] studied the amplification of both deep and shallow deposits for 1D and 2D models. Campillo *et al.*[6] computed the response to Lg waves (trapped S-waves) of a sedimentary basin with similar characteristics to the deep basin beneath Mexico City, finding an amplification of 5 and reproducing the signals at hill zone sites. Paolucci and Faccioli[9] used an exact 2D solution for wedge-shaped alluvial layers and compared time-domain results with real accelerograms. Pérez-Rocha *et al.*[11] and Sánchez-Sesma *et al.*[12] studied in detail data from recent earthquakes and compared them with results from axisymmetric configurations. Kawase and Aki[13] studied the long duration observed in the valley suggesting that it is caused by the interaction of soft-surface layers with a deep basin structure. Singh and Ordaz[14] used the 1D model and data from the recently installed broad-band seismograph to explain the large duration observed at lake-bed zones stating that this duration has always been present in the excitation, but the accelerations did not reach the necessary threshold for the standard instruments at hill zone sites to continue the recording. Chávez-García and Bard[15] took a comprehensive look at site effects for the 1985 earthquake, examining 1D and 2D models. Ordaz and Faccioli[16] modelled with the 1D method the non-linear response of the southern Xochimilco-Chalco lake. Finally, a hybrid technique was used[17] to take into account source, path and local soil effects, showing that the large durations observed are due to the resonance effects and the excitation of local surface waves in the laterally heterogeneous layer; in this work the motion in the valley along a cross-section was simulated and the results were compared with data only from the 1985 earthquake and, unfortunately, not with recent data recorded since 1988 by the network.

The method employed in this work is the direct boundary element method based on integral equation formulations of the continuum mechanics.[18] The unknowns and boundary conditions are displacements and tractions which are approximated over the elements from its values at the nodes using interpolation functions. The method is very attractive for wave propagation problems because the discretization is done only on the boundary, yielding smaller meshes and systems of equations. The price to be paid is that the system of equations is non-symmetric and fully-populated, leading to longer computer times. Another advantage is that this method represents efficiently the outgoing waves through infinite domains, which again is very useful when dealing with scattered waves by topographical structures. The method has been used previously[4,13,19–23] and only the main contributions of this work are presented.

Although the 1D theory can explain most of the observed amplification in the city, 2D and 3D models are needed to explain the amplification behaviour at the edges of the valley and at the sites where the clay deposit is deeper.[24–26] The 1D model was applied to a site that is representative of a large area of the lake-bed zone,

while the 2D model was used to model a section of the valley where irregular response has been observed and which was suitable to be modelled with a 2D section.

THE DIRECT BOUNDARY ELEMENT METHOD

The geometry of the problem under consideration is shown in Figure 1 where the incident wave is either a P-, SV- or a Rayleigh wave. The domain Ω is the 2D half-space below the infinite traction-free boundary Γ. The medium is assumed to be homogeneous, linearly elastic and isotropic. The propagation of harmonic P-, SV- and Rayleigh waves in Ω is described by the Navier–Cauchy equations. Applying the principle of superposition, the vector of displacements $\mathbf{u}$ can be written as

$$\mathbf{u} = \mathbf{u}_s + \mathbf{u}_0 \tag{1}$$

where $\mathbf{u}_s$ is the contribution of the scattered wave due to the presence of the irregularity Γ_s and $\mathbf{u}_0$, the so-called free-field displacement, is the analytical solution of a wave propagating on a half-space. The displacement $\mathbf{u}_s$ satisfies the Sommerfeld radiation condition and is defined by the following Navier–Cauchy integral representation formula[18]

$$c_{lk}(\zeta)\, u_{s_k}(\zeta) = \int_\Gamma p_{s_k}(\chi)\, u^*_{lk}(\zeta,\chi)\, \mathrm{d}\Gamma(\chi) - \int_\Gamma u_{s_k}(\chi)\, p^*_{lk}(\zeta,\chi)\, \mathrm{d}\Gamma(\chi) \tag{2}$$

valid for every $\zeta \in \Omega$ and the integrals are in the sense of Cauchy principal value. Index l refers to the direction of the load producing displacements or tractions in the k direction. The matrix c_{lk} contains non-complex constants which depend on the boundary geometry and its orientation with respect to the global co-ordinates system. This 2×2 matrix is usually computed assuming rigid-body motion. Unfortunately, for a half-space such considerations do not apply and therefore c_{lk} has to be computed explicitly as a function of the internal angle of the boundary subtended at ζ. The expression[26] is

$$c_{lk} = \frac{1}{8\pi(1-\nu)} \begin{bmatrix} 4(1-\nu)\vartheta_0 + \sin 2\vartheta_1 - \sin 2\vartheta_2 & \cos 2\vartheta_2 - \cos 2\vartheta_1 \\ \cos 2\vartheta_2 - \cos 2\vartheta_1 & 4(1-\nu)\vartheta_0 - \sin 2\vartheta_1 + \sin 2\vartheta_2 \end{bmatrix} \tag{3}$$

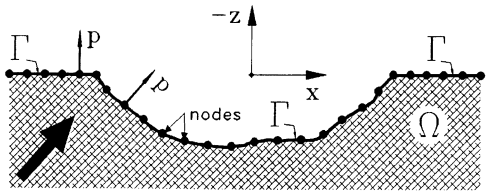

Figure 1. Scattering by canyons for P-, SV- and Rayleigh waves using the boundary element method

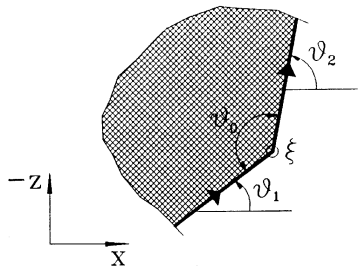

Figure 2. Geometrical definitions for the computation of **c**

where v is Poisson's ratio and ϑ_0, ϑ_1 and ϑ_2 are the angles shown in Figure 2. When the boundary is smooth at ζ, $c_{11} = c_{22} = \frac{1}{2}$ and $c_{21} = c_{12} = 0$.

The kernels $u^*_{lk}(\zeta, \chi)$ and $p^*_{lk}(\zeta, \chi)$ of equation (2) are the 2D fundamental displacement and tractions of steady-state elastodynamics for an unbounded region. When the source point ζ, lies on the same element as the integration point χ, the integrals in equation (2) become singular. The first integral of this equation is weakly singular and is solved with a special integration using a logarithmic Gaussian quadrature.[18] The second integral in equation is strongly singular because $p^* = O(1/r)$. A special treatment[18] can be given to this integral: the dynamic tractions p^* can be written as

$$p^* = p_{ss} + p^*_s \tag{4}$$

where p^*_s are the tractions for the static fundamental solution and p_{ss} is a regular series obtained with the difference between the dynamic and static fundamental solutions; p_{ss} tends to zero as the frequency tends to zero.[18] Thus, the steady-state dynamic solution will tend to the static as the frequency tends to zero and the singularity now is the static one which is explicit and easier to calculate than the dynamic one. This singularity can be evaluated either by applying rigid-body motion[18] or by evaluating the Cauchy principal value integral as has been done in this work.

At any point on the boundary Γ, surface force intensities or tractions are produced by the stress components. The solution of equation (2) has to satisfy the traction-free condition for the total traction at Γ. Because of the principle of superposition, it is possible to write

$$\mathbf{p}_s = -\mathbf{p}_0 \tag{5}$$

where the tractions $\mathbf{p}_0$ and $\mathbf{p}_s$ are produced by the incident and the scattered wave, respectively. The expressions for $\mathbf{p}_0$ are obtained with the stress tensor produced by the free-field $\mathbf{u}_0$.[26]

Applying the method of collocation using the nodes as collocation points,[18] equation (2) becomes, for every ith node,

$$\mathbf{c}^i \mathbf{u}^i_s + \sum_{j=1}^{N} \left\{ \int_{\Gamma_j} \mathbf{u}^i_s \mathbf{p}^* \, d\Gamma \right\} - \sum_{j=1}^{N} \left\{ \int_{\Gamma_j} \mathbf{p}^i_s \mathbf{u}^* \, d\Gamma \right\} = 0 \tag{6}$$

where Γ_j is the surface of the jth element, $\mathbf{u}^*$ and $\mathbf{p}^*$ are 2×2 matrices of the fundamental displacements and tractions, respectively, and $\mathbf{u}^i_s$ and $\mathbf{p}^i_s$ are the vectors of displacements and tractions for each node. Writing the variation of $\mathbf{u}^i_s$ and $\mathbf{q}^i_s$ in terms of interpolation functions and nodal values and considering the contribution for all i nodes, equation (6) can be written in matrix form to give the global system of linear equations

$$\mathbf{H}\mathbf{u}_s - \mathbf{G}\mathbf{p}_s = 0 \tag{7}$$

where $\mathbf{H}$ and $\mathbf{G}$ are non-symmetric square matrices and $\mathbf{u}_s$ and $\mathbf{p}_s$ are vectors, all of order $2 \times N$. For the case of canyons (Figure 1), because of the traction-free boundary condition (equation (5)), the above equation can be written as

$$\mathbf{H}\mathbf{u}_s = -\mathbf{G}\mathbf{p}_0 \tag{8}$$

Once $\mathbf{u}_s$ is obtained, total displacements $\mathbf{u}$ will be given by equation (1).

Consider now the two regions shown in Figure 3: the half-space Ω_h and the valley Ω_v. Assume that the respective displacements fields are $\mathbf{u}_h$ and $\mathbf{u}_v$. In Ω_h, the displacement $\mathbf{u}_h$ and the traction $\mathbf{p}_h$ are obtained in the same way as for canyons. For both regions, the traction-free boundary condition applies at $z = 0$:

$$\mathbf{p}_h = \mathbf{p}_v = 0 \tag{9}$$

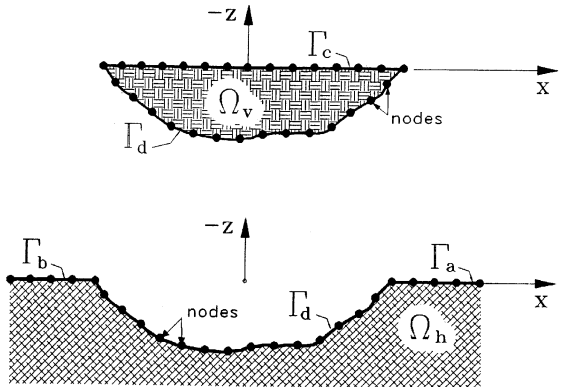

Figure 3. Scattering by valleys for P-, SV- and Rayleigh waves using the boundary element method

where $\mathbf{p}_v$ is on Γ_c and $\mathbf{p}_h$ is on Γ_a and Γ_b. Therefore, for these boundaries, equation (5) is still valid. Due to the matching conditions, the tractions $\mathbf{p}_h$ on Γ_d are now unknown.

Displacements and tractions for the half-space due to the scattered wave, can be obtained according to Figure 3 by the following matrix system:

$$\mathbf{H}_h[\mathbf{u}_s^a + \mathbf{u}_s^d + \mathbf{u}_s^b] - \mathbf{G}_h[\mathbf{p}_s^a + \mathbf{p}_s^d + \mathbf{p}_s^b] = 0 \tag{10}$$

On the other hand, total displacements and tractions of the valley are given in terms of the internal wave that satisfies equation (2) but is not required to satisfy the radiation condition. They can be computed from the following system of equations:

$$\mathbf{H}_v[\mathbf{u}_v^c + \mathbf{u}_v^d] - \mathbf{G}_v[\mathbf{p}_v^c + \mathbf{p}_v^d] = 0 \tag{11}$$

where the total tractions $\mathbf{p}_v^c = 0$ (equation (9)).

Because the traction-free condition applies on Γ_a and Γ_b (equation (9)) and using the compatibility and equilibrium conditions at the interface Γ_d, the resulting system from equations (10) and (11) is

$$\begin{bmatrix} \mathbf{H}_h & \mathbf{H}_h & \mathbf{H}_h & 0 & -\mathbf{G}_h \\ 0 & \mathbf{H}_v & 0 & \mathbf{H}_v & \mathbf{G}_v \end{bmatrix} \begin{bmatrix} \mathbf{u}_s^a \\ \mathbf{u}_s^d \\ \mathbf{u}_s^b \\ \mathbf{u}_v^c \\ \mathbf{p}_s^d \end{bmatrix} = \begin{bmatrix} -\mathbf{G}_h & \mathbf{p}_0^a & -\mathbf{G}_h & \mathbf{p}_0^b \\ -\mathbf{H}_v & \mathbf{u}_0^d & -\mathbf{G}_v & \mathbf{p}_0^d \end{bmatrix} \tag{12}$$

with $\mathbf{u}_s$, $\mathbf{u}_v$ and $\mathbf{p}_s$ unknowns. Total displacements $\mathbf{u}_v$ at the surface of the valley are given by solving the above system while total displacements for the half-space are given by equation (1). Although equation (12) is valid only for two regions, the half-space and the valley, the approach is general and applicable to several regions (i.e. the half-space and strata inside the valley).

Finally, equations (8) and (12) can be written in general form as

$$\mathbf{A}\mathbf{x} = \mathbf{b} \tag{13}$$

where the matrix $\mathbf{A}$ does not depend on the type of incident wave or boundary conditions. This means that, for a given topography or valley with certain geometry and properties, the solution for P-, SV- and Rayleigh

waves (and for as many incident angles as desired) could be obtained in just one step with a minimum of extra time. For this case, instead of a vector **b**, a matrix **B** is used. In this way, each column of **B** represents the boundary conditions for a given wave with a certain incidence angle.

The method was tested against results of other numerical methods and for a wide range of problems.[26] With a few quadratic boundary elements in the irregularity and in the surface of the half-space, the method can be used to obtain reliable results of the scattering from topographical features and alluvial valleys as long as there are at least 4 quadratic elements per wavelength. The free surface Γ_a and Γ_b of Figure 3 has to be discretized with a finite number of boundary elements. This finite discretization introduces a truncation and, therefore, an error that could be minimized if an appropriate length of discretization is chosen. A parametric study[26] shows that this length of discretization is not relevant for most applications (considering actual material properties of the valley of Mexico) if the solution is required at the surface of the valley or canyon. Even for low frequency, errors obtained for the length of $2a$ (a being the radius of the canyon) were smaller than 10 per cent compared with the exact solution, which suggest that there is no need to discretize long lengths of the free-surface. Because of this relatively short length needed for the discretization, together with the difficulty to formulate and solve the Green's functions for dynamics for the half-space,[22] no image solution was employed.

OBSERVED AMPLIFICATION IN THE MEXICO CITY VALLEY

Mexico City Valley and accelerometric network

Mexico City is located on a valley approximately 110 km long and 80 km wide. The valley is completely surrounded by mountains, some of which reach up to 5230 m over the sea level. The lowest part of the valley has an altitude of 2230 m. Figure 4 shows the southwest part of the valley where the city is located. Some reference sites and main streets are indicated, as well as accelerometric stations and the three main geotechnical zones: (I) hill zone, localized in the higher parts of the valley, formed by hard soils of high resistence; (II) transition zone, with mixed characteristics of the hill and lake-bed zones; (III) lake-bed zone, consisting of very soft and compressive alluvial deposits, where shear wave velocities can be as low as 50 m/s and the water content up to 400 per cent.

Since 1965, accelerometric data in the city have been obtained, from a wide range of earthquakes with different magnitudes (M) and epicentral distance (R), at a hill-zone site (CU, *Ciudad Universitaria, UNAM*) south of the city. During the devastating Michoacán earthquake in 1985 ($M = 8{\cdot}1$, $R = 400$ km) data were collected at 11 sites; unfortunately, only site SC recorded data from the zone of damage in the city. This record alone provided an important precedent of the amplification that can be observed in alluvial valleys such as the one in Mexico City. With a larger network of more than 100 digital accelerometers, enormous amounts of data have been collected since 1986 from more than 16 small and moderate subduction earthquakes ($4.5 < M < 7.5$), all of them with a range of distance from their rupture area to CU between 250 and 500 km.

Spectral ratios between hill and lake zones

The motion observed at the Mexico City Valley is one of the best examples of dynamic amplification in alluvial basins. At some frequencies, this amplification could be as large as 500 times with respect to the registered at near-source stations.[27]

The dramatic way in which site effects manifest in Mexico City is mainly due to the high contrast between the dynamic characteristics of the alluvial strata and the bed rock. In the frequency domain, the form of the amplification is controlled by the elastic impedances, damping of the soil, characteristics of the incident field and the geometry of the valley. In the time domain this response manifests in harmonic motions and in larger amplitude and duration of the records.

Accelerometric data from subduction earthquakes were used by Singh *et al.*[27] to obtain the empirical amplification of the Mexico City Valley. They computed empirical transfer functions or spectral ratios in order to obtain the measured amplification at transition and lake-bed zone sites with respect to CU, finding some differences in the amplification patterns that were not satisfactorily explained.

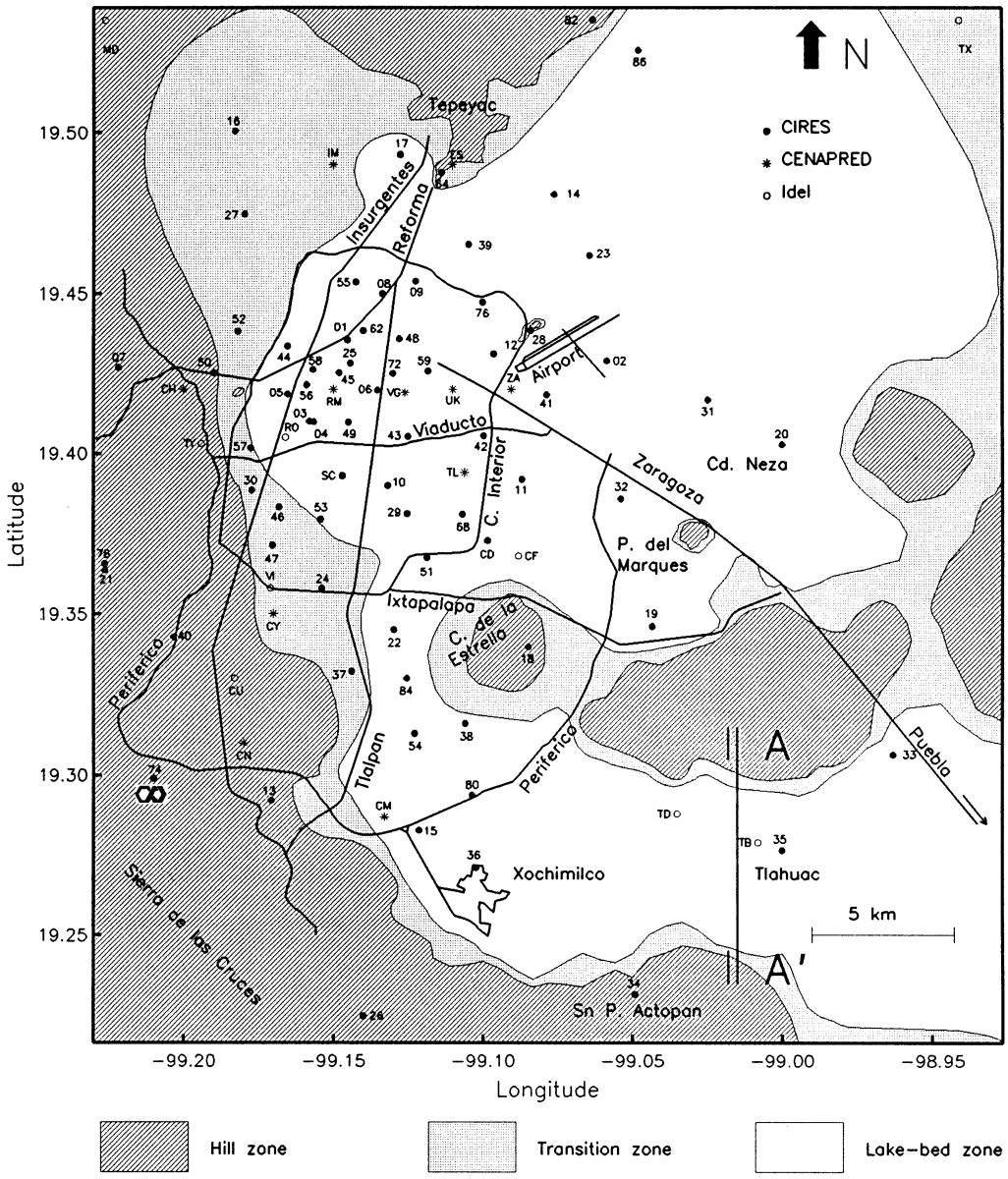

Figure 4. Mexico City Valley: accelerometric stations, main streets, reference sites and geotechnical zones

In order to study with more detail these ratios, a later study[24] observed that the amplification obtained at more than 80 per cent of sites was practically the same for all earthquakes, no matter their magnitude, distance or azimuth. This was possible because of the incorporation of data of recent earthquakes, the selection of data considered reliable (as spectral ratios are very much dependent on the noise-to-signal ratio), and the use of the average Fourier amplitude spectra at hill-zone sites as the reference site. This conclusion was also valid for the earthquake of 1985 in which important non-linear behaviour did not seem to be present.[16,24,27]

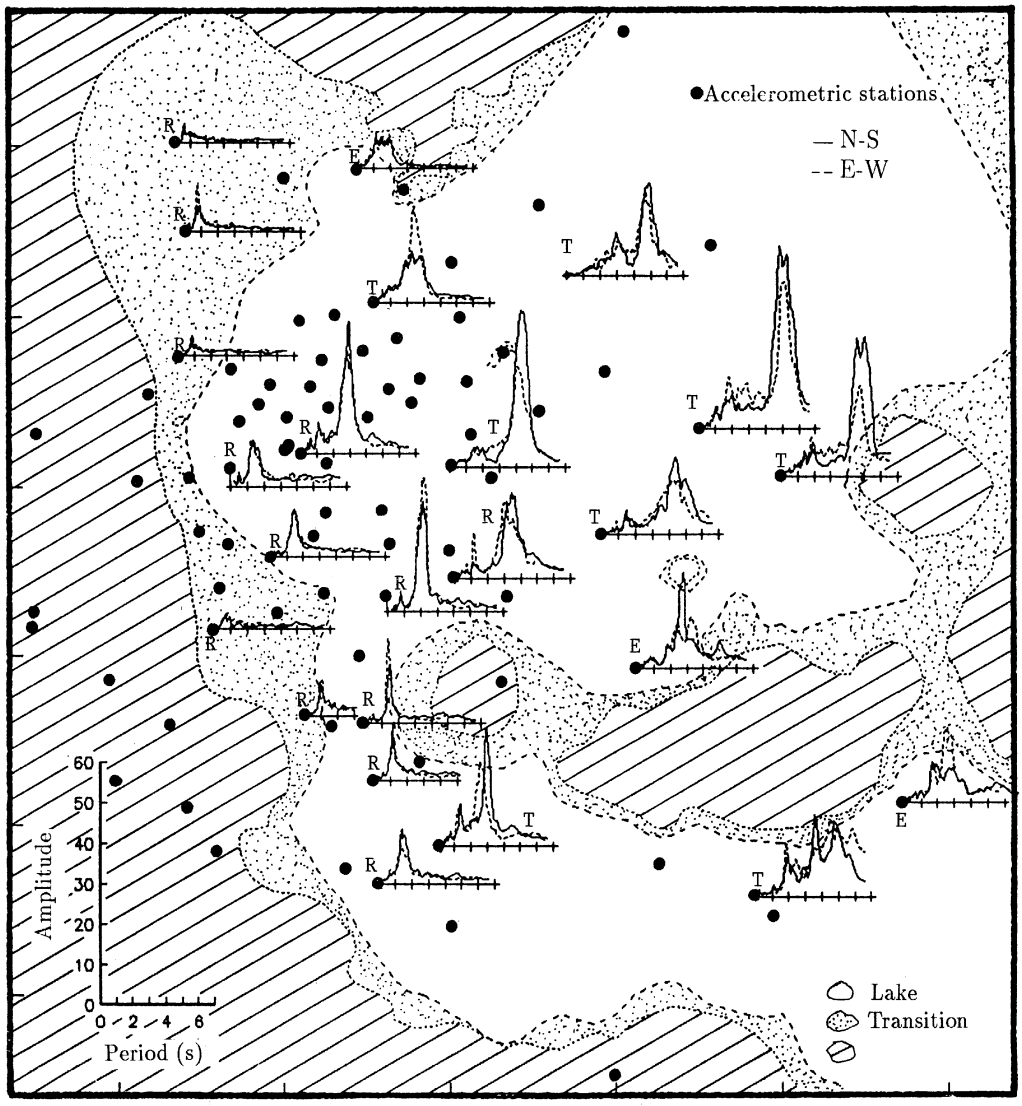

Figure 5. Some average ratios of all earthquakes and horizontal components indicated with an *R*, if showing a regular response, with a *T*, if located over thick alluvial deposits, or with an *E*, if located near the edges of the lake-bed zone

The idea of using the average Fourier spectra at hill-zone sites is because strong motions there exhibit important differences from one site to another during the same earthquake[25,26] but, on average, their behaviour in the frequency domain is fairly similar. This is valid only for hill-zone sites located over recent Cuaternary deposits (07, 13, 21, 34, 40, 50, 74, 78, CU and TY, Figure 4). The different response among these stations could be due to topography site or regional effects, vertical propagation of body waves trough slightly different strata or to randomness. Up to now, topography effects have been difficult to be quantified[26,28] because 2D and 3D models need to be used; on the other hand, vertical propagation models need reliable field and laboratory studies to define the properties of the strata. Thus, having used the average spectrum, the differences observed among hill-zone sites are considered as random, as topography and different vertical propagation effects are supposed to be small and were not taken into account. Therefore, for each earthquake and component of

motion, we take the average Fourier spectrum of sites located over Cuaternary deposits as representative of the motion at hill zone.

From the spectral ratios results,[24–26] it has been shown that most lake and transition sites behave as the 1D model predicts and, therefore, are considered as having regular response. However, at some sites near the edges of the valley (17, 19, 33, CF and TD, Figure 4) and some sites over the most thick alluvial deposits (02, 09, 11, 12, 14, 20, 23, 31, 32, 35, 36, 41, 42, 80, CD, TB and ZA, Figure 4) the ratios show responses that suggest 2D and 3D effects; this is because the ratio is systematically different for both horizontal components of for different earthquakes. Figure 5[25] depicts some average ratios (considering all earthquakes) of both horizontal components; they are indicated with an *R*, if showing a regular response, with a *T*, if located over thick alluvial deposits, or with an *E*, if located near the edges of the lake-bed zone.

ONE-DIMENSIONAL RESPONSE OF THE MEXICO CITY VALLEY

Because the soft alluvial layer in Mexico City is relatively flat and shallow, it is easy to agree that the 1D theory is enough to explain the amplification patterns. Moreover, the high contrast of S-waves between the clays and the basement rock also favours the use of simple, 1D wave propagation models.

The 1D model for vertically incident S-waves has been the only analytical method actually employed to predict the amplification of the seismic motion at lake-zone sites. This was the case of the design spectra included in the 1987 seismic code that was obtained with 1D results[29] using CU as reference station. In some works, this model has been successfully used to reproduce average ground motion characteristics for Mexico City. Romo and Seed[30] have obtained the response spectra at various locations of the valley using random vibration theory and 1D wave propagation models. Seed *et al.*[31] presented a study using 1D models concluding that they allowed to obtain a very good match of observed response spectra for the 1985 earthquake. Kawase and Aki[13] justified the use of 2D models showing that the model of Seed *et al.*[31] was accurate for response spectra but not for spectral ratios computed for sites SC and CD for the 1985 earthquake; they also concluded that the 1D model did not explain all the amplification patterns observed during the earthquake. Chávez-García and Bard[15] compared the response at one site for the 1989 earthquake with a 1D model, finding a good agreement in the frequency domain but not in the time domain. Bard *et al.*[5] showed, with a 2D model, that the amplification patterns at the centre of the valley could be very similar to the 1D results, but at the edge of the lake an irregular amplification should be expected. Ordaz *et al.*[32] analysed bore-hole recordings finding an excellent agreement between the observed amplification and the 1D model. Ordaz and Faccioli[16] used the 1D approach to study the non-linear response of two sites of the southern Xochimilco-Chalco lake.

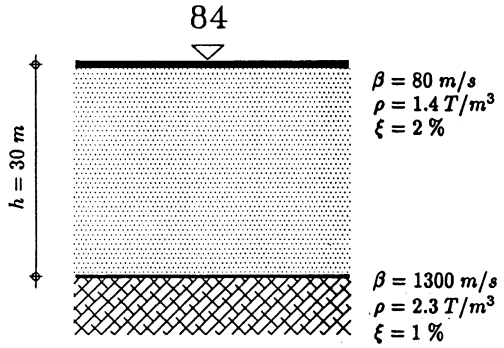

Figure 6. Profile used to obtain the 1D response at site 84

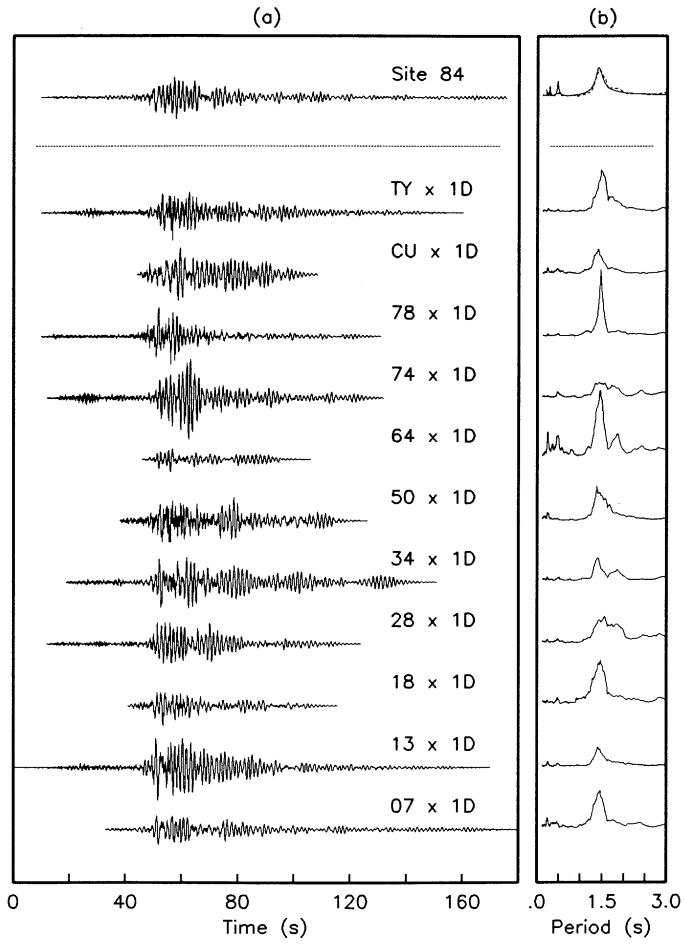

Figure 7. Response at site 84 for the north-south component of motion during the 1989 earthquake: (a) Recorded accelerogram (top) and one-dimensional time responses using all hill zone sites that recorded the earthquake. (b) One-dimensional transfer function and average ratio (top) with solid and dashed lines, respectively, and spectral ratios between each hill-zone site and site 84

As a typical example of 1D behaviour we have chosen site 84.[25] The area where this station is located is now considered as a high-intensity seismic zone. The characteristics of motion at site 84 are very similar to its surrounding stations (22, 37 and 54, Figure 4) and therefore all the following studies regarding 84 are also applicable to the others.

With a simple 1D geometry (Figure 6) and the Haskell method, we have computed the 1D response at site 84 with data of the north–south (NS) component of motion recorded during the 1989 earthquake ($M = 6{\cdot}9$, $R = 300\,\text{km}$) using each of the 11 hill-zone accelerometric stations as reference sites. The comparison between these 1D responses with the recorded accelerogram at site 84 is shown in Figure 7(a). The right part of this figure (Figure 7(b)) shows the spectral ratio between the respective hill-zone site and site 84; at the top of Figure 7(b), the average spectral ratio (dotted line) and the 1D transfer function (solid line) are also shown. Although important differences can be seen for each reference station in both frequency and time domains, we argue that site 84 exhibits 1D response because the average ratio is almost identical to the 1D transfer function.

The differences computed for each station have reasonable explanations only for sites 18, 28 and 64, which are located over old (Terciary) features of the valley and have systematically lower or different amplitude.

Apart from these three reference stations, we believe that most differences observed in Figure 7 could be attributed to random or noise contributions to the strong ground motion at hill zone sites which disappear when calculating the average motion as stated in previous paragraphs.

From these results, it is clear that, in average, the 1D model can reproduce with good accuracy the amplification patterns observed at site 84 for a moderate earthquake. But it is also clear that, if we isolate some of these results, they can be used to argue against the efficiency of the 1D theory just by stressing the differences in the time domain (lower or larger amplitudes, shorter durations, different phases and larger harmonic codas) or in the frequency domain (different amplitude and frequency content). These different amplification patterns (Figure 7) illustrate the importance of selecting a reference site to study the lake-bed zone behaviour, as has been already published by Reinoso *et al.*[25] and latter by Ordaz and Faccioli.[16]

The relatively high level of acceleration that could have taken place during the earthquake of 1985, together with the large duration of the strong motion, are enough reasons to explain the structural damage observed at this zone of the city. Thus, we think that there is little place for other explanations of the damage like trapped waves between hill zones.[33] Comparisons with data from other earthquakes[26] show that the azimuth does not affect the response at this site, an amplification pattern which is valid only, in general, for 1D behaviour.

TWO-DIMENSIONAL MODELLING USING THE DIRECT BOUNDARY ELEMENT METHOD

Site TB

Among sites that have been exhibiting irregular response, site TB was chosen to be presented as an example of possible 2D behaviour. Site TB is located at the centre of the alluvial deposit (Figure 4) over strata of more than 100 m of very soft clay. It was chosen because the spectral ratios for this station are very different for both horizontal components and for all earthquakes, so the average ratio presents large standard deviations.

Figure 8 shows the ratios computed for site TB for the 1985 (Figure 8(a)) and 1989 (Figure 8(b)) earthquakes with respect to sites CU (continuous line), TY (dashed line) and the average Fourier spectra at hill-zone sites (dotted line); also shown are the accelerometric records. From Figure 8 it can be observed that results for both horizontal components of each earthquake differ considerably, a strong evidence of 2D and 3D response. Moreover, the different shape of the ratios for both earthquakes suggest that site TB could be very sensible to the azimuth of the earthquake: the 1989 earthquake came strait from the south (azimuth $= 186°$) while the 1985 earthquake came from the southwest (azimuth $= 240°$) that could have cause, due to the canal-type geometry of the valley (Figure 4), 3D amplification patterns in this zone. Because of these probable 3D effects, data from the 1985 earthquake were not used.

Figure 9 is another evidence that the 1D model does not explain the behaviour at site TB. Figure 9(a) depicts the observed accelerogram of the NS component registered during the 1985 earthquake and two simulated accelerograms using the 1D model and CU and TY as reference stations. It has been assumed that these two reference stations have the same characteristics of the input motion beneath TB. The comparison of the accelerograms looks quiet satisfactory, but, at the top of the figure, it is shown that the dominant period computed along the observed accelerogram (obtained from the smooth amplitude Fourier spectra of a moving 30 s window) changes from 3·6 to 5·4 s, while the simulated accelerograms always present the 1D dominant period (5·2 s). The same shift of dominant period is observed for the 1989 earthquake (Figure 9(b)), although the simulated accelerograms are quiet different compared with the observed motion.

Another reason to select site TB in this study is because it was the easiest place to propose a relatively simple (in shape and size) 2D geometry with rough characteristics of the actual valley. The section modeled is the A–A′ section of Figure 4 and the geometry used to represent it was a 5 km wide and 150 m deep parabolic valley (Figure 10). This geometry was chosen after trying with several 2D flat valleys with differents slopes at the borders that yielded responses at the center very similar to the 1D response. The velocity and mass density ratios between the half-space and the valley were 13 and 2, respectively, the damping and Poisson's

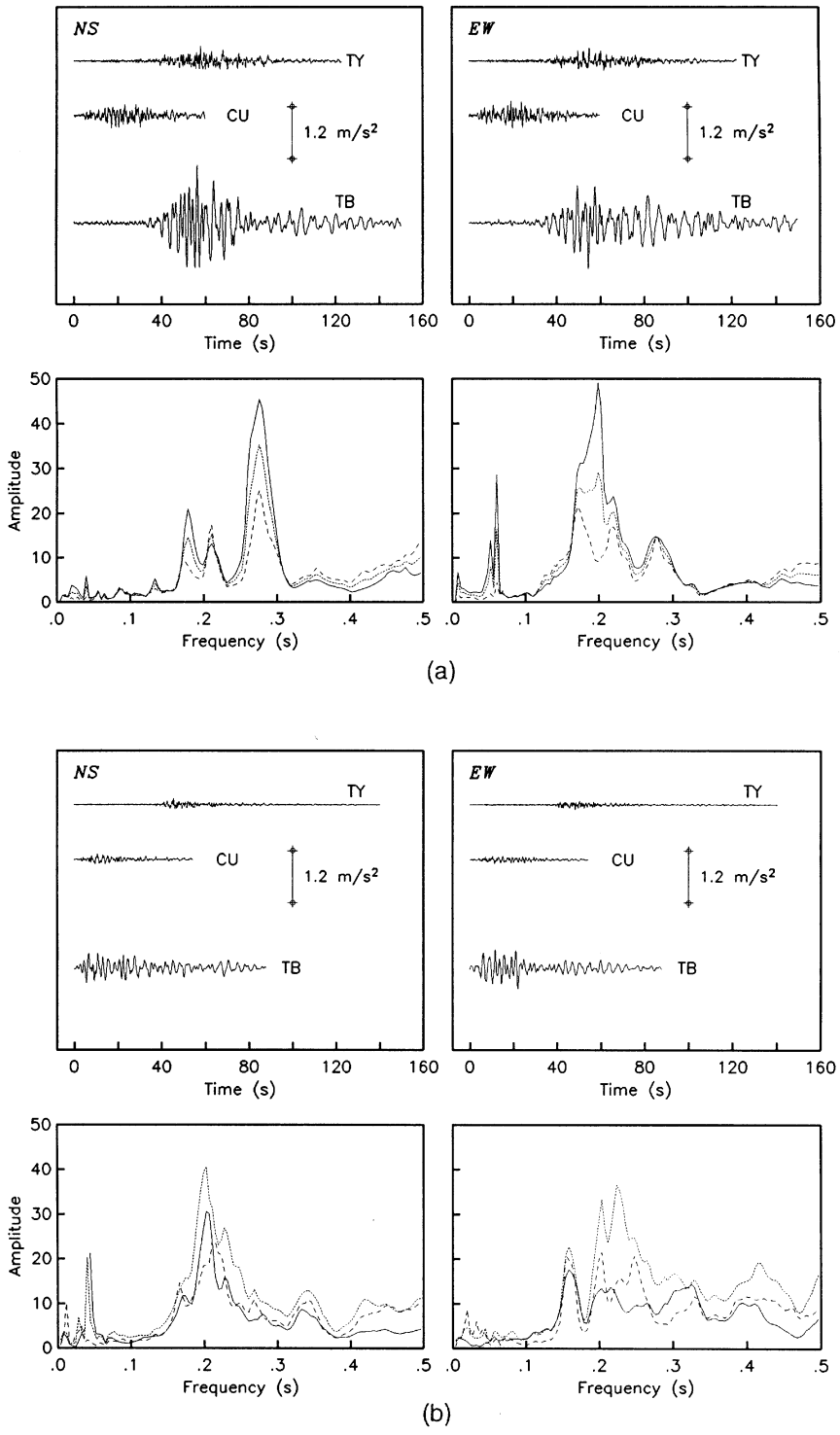

Figure 8. Ratios computed for site TB with respect to sites CU (continuous line) and TY (dashed line); also shown are the transfer function with respect to the average Fourier spectra at hill-zone sites (dotted line) and the accelerometric records: (a) 19 September 1985 earthquake; (b) 25 April 1989 earthquake

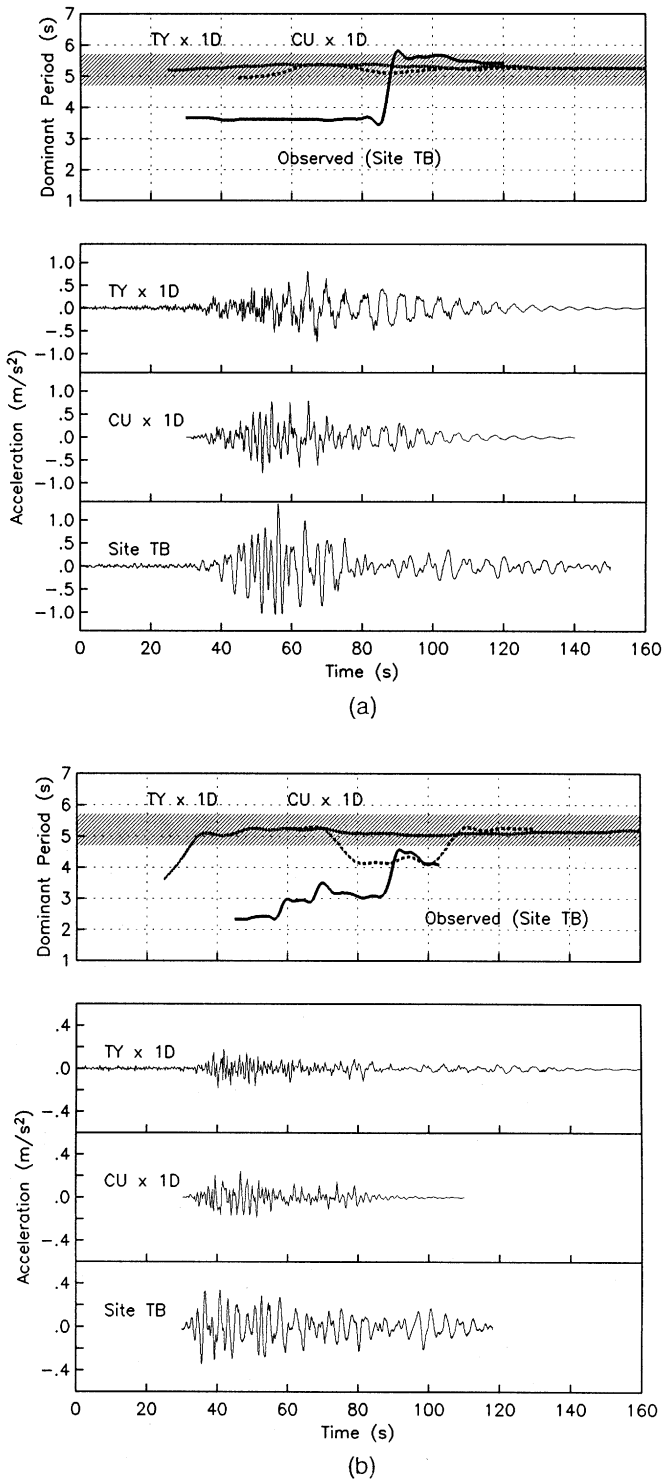

Figure 9. Observed accelerograms of the NS component and two simulated accelerograms using the 1D model and CU and TY as reference stations. At the top of the figure, the dominant period computed along each accelerogram is also shown: (a) 19 September 1985 earthquake; (b) 25 April 1989 earthquake

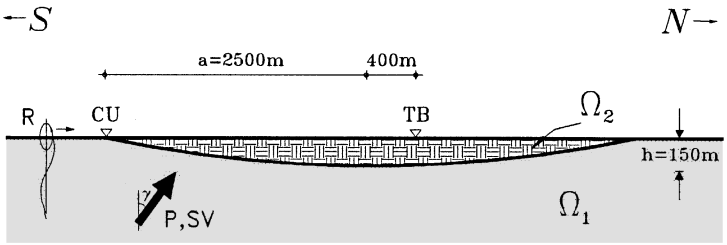

Figure 10. Two-dimensional section used to model the response at site TB (line A–A′ of Figure 4)

ratio of the material inside the valley were 2 per cent and 0.495, whereas damping, Poisson's ratio and S-wave velocity of the bed-rock were 1 per cent, $\frac{1}{3}$ and 1300 m/s^2, respectively. Damping or viscous decay in the scattering wave has been considered using complex wave numbers of the form $k'_\beta = k_\beta(1 - \mathrm{i}D)$ where D is the constant hysteretic factor in per cent. The 1D response of this site was computed using the above properties considering a flat valley 145 m deep.

Accelerometric station CU has been the reference site most widely used since an accelerometric station was installed there in 1964. Dozens of works for different purposes have used CU as reference station. As has been stated in this work, only sites over Cuaternary deposits should be used as reference sites. In order to compare the numerical results with the recorded data, site CU (located over 2000 yr old lavas) was chosen as reference site as previous studies have probed that it is the best choice to study the amplification at TB.[16,25] Moreover, not only CU was chosen considering the relative position of the A–A′ section of Figure 4, but also because the spectral ratio of site TB with respect to CU is very similar to the ratio computed for TB with respect to the average hill-zone sites motion (Figure 8).

Incident SH-waves

Reinoso *et al.*,[25] obtained transfer functions from the model shown in Figure 10 for incident SH-waves. It was shown that the 2D results can reproduce some of the amplification patterns that the 1D theory is not able to predict. Although these results did not have the purpose of reproducing every feature of the response at TB, they clearly showed that the predictions of a rough 2D model were far closer to the observations than those of the 1D model. At least for the geometry studied, the angle of incidence did not seem to be a relevant factor in the response of the valley.

It was also concluded that time domain simulations for sites in Mexico City with large dominant periods ($T > 2{\cdot}0$ s) and therefore long responses, are still difficult to match with observations owing to the short duration registered at the reference sites. It is believed that 2D and 3D effects contribute significantly to the large duration of the records. But it is also true, as was pointed out by Singh and Ordaz,[14] that the most significant part of the duration can be explained by the 1D theory, provided that the register at the reference site is as long as that at the lake-zone site (as shown in Figure 6 for site 84).

Incident P-, SV- and Rayleigh waves

Using the 2D boundary element formulation for elastodynamics presented in this work, we modelled the same 2D configuration[25] but now focused on the NS component of motion. Transfer functions for incident P-, SV- and Rayleigh waves were obtained on the surface of the valley at and near the observation point TB of Figure 10. Figure 11 shows these transfer functions for P-, SV- and Rayleigh waves. For P-waves, results for incident angles of 45, 30 and 15° are shown from top to bottom, while for SV-waves results for incident angles of 30, 15 and 0° are shown in the same order; plots on the left, centre and right sides, correspond to results at the surface points $x = 100, 400$ and 700 m, respectively.

The smooth spectral ratio between TB and CU obtained with the NS components of the 1989 earthquake is shown in Figure 12. Figure 13 shows the 1D response for vertically incident SV-waves of the site TB

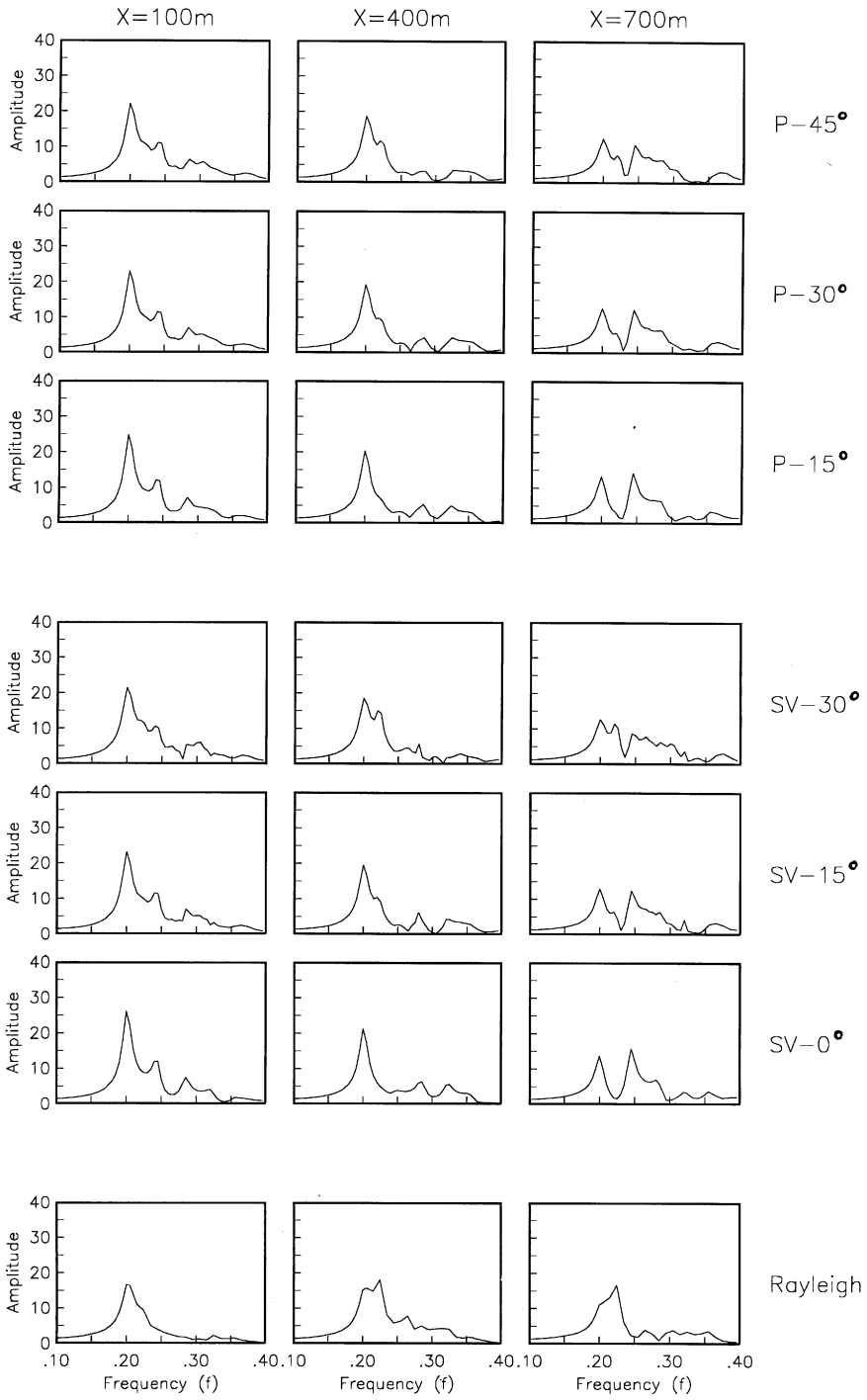

Figure 11. Two-dimensional response due to incident P-, SV- and Rayleigh waves, at three observations points ($x = 100, 400$ and 700 m) on the surface of the valley shown in Figure 10. For P- and SV-waves, three different incidence angles are shown

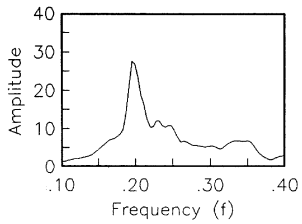

Figure 12. Spectral ratio of the north–south component between CU and TB

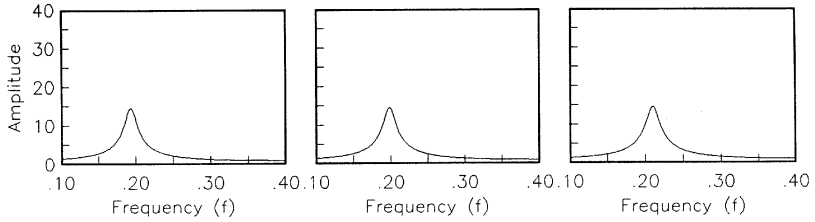

Figure 13. One-dimensional transfer function for vertically incident S-waves at $x = 100, 400$ and 700 m

($x = 400$ m) and for other two sites near TB ($x = 100$ and $x = 700$ m) computed using the same properties of the valley at the corresponding depths of 145, 149 and 138 m.

As can be appreciated in these figures, for the point at $x = 400$ m, the 2D response for P- and SV-waves is closer to the spectral ratio than the 1D response. For non-vertical incidence some peaks appear that are also observed in the spectral ratio. However, the ratio has larger amplitude than the 2D responses. For the other two observation points, 2D modelling shows amplification patterns very different from those of the 1D theory, mainly for the site at $x = 700$ m. The response due to incident Rayleigh wave is very similar to the 1D response.

From these 2D results, it is possible to say that the proposed geometry of the valley yields a response that is close to the one observed at site TB during the 1989 earthquake using CU as a reference site. However, these results have mainly a qualitative significance, and show that site TB has been exhibiting important 2D, and possibly, 3D effects.

Time–responses using a Ricker's wavelet are shown in Figures 14–16. For P-waves, Figure 14(a) corresponds to a wavelet with 5 s period and 30° incidence, while Figure 14(b) corresponds to a wavelet of 3 s and 75° incidence. For SV-waves, Figure 15(a) shows a wavelet with a period of 3 s and 30° incidence and Figure 15(b) shows a wavelet of 5 s and vertical incidence. Time–responses for Rayleigh waves are shown in Figures 16(a) and 16(b) for wavelets of 3 and 5 s, respectively.

From Figures 14–16 it can be observed that the amplification pattern is quite similar for all incident waves. This can be due to the fact that this amplification is governed by the same P–S conversion for all types of waves and incidences, which implies that the valley, or at least the geometry studied, is not sensitive to these changes.

Finally, Figure 17 shows the 1D time–response of a vertically incident S-wavelet for the corresponding TB site ($H = 145$ m). It is clear that even the 1D model predicts large amplification in both amplitude and duration, although 2D responses show latter arrivals that make the code slightly larger than the 1D results.

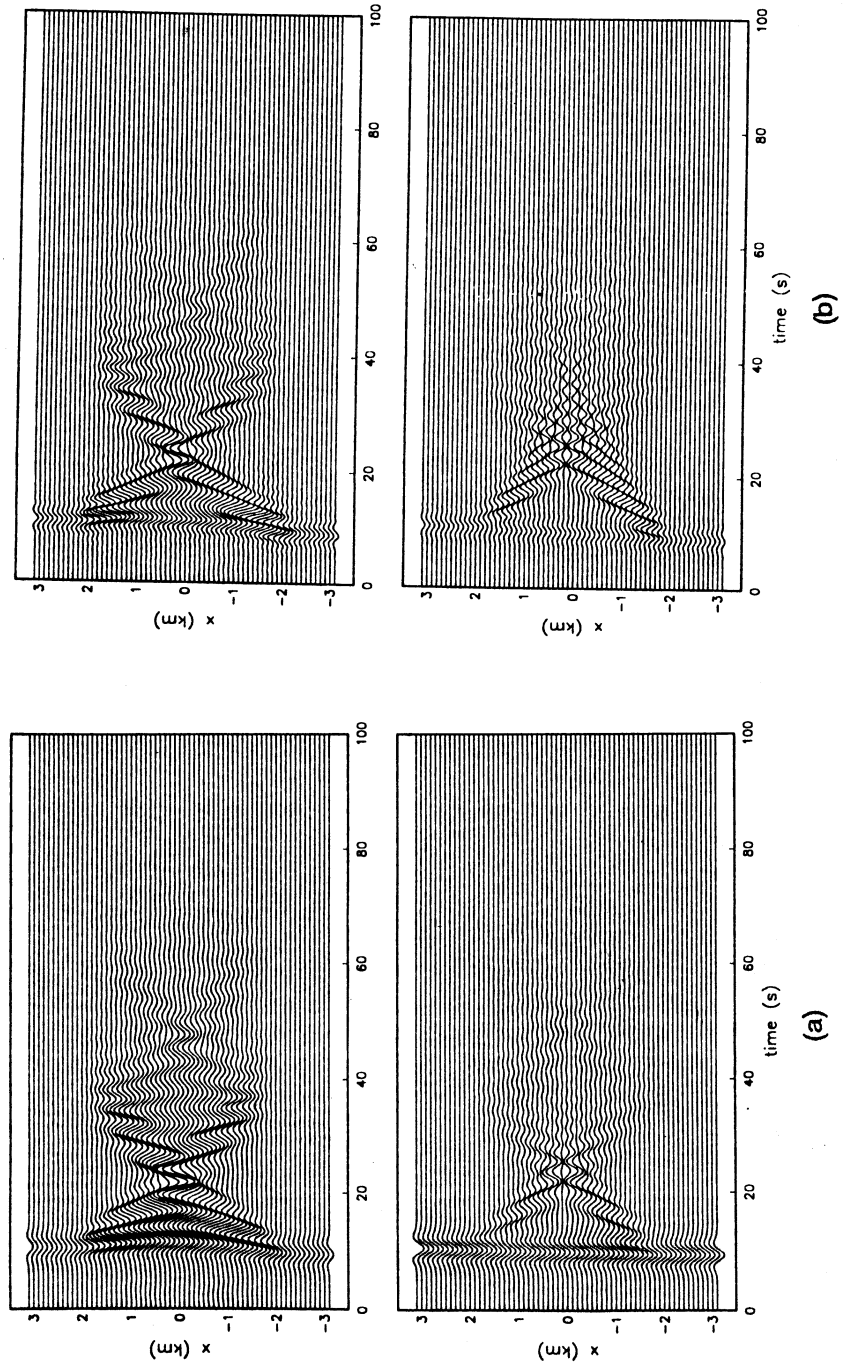

Figure 14. Time–responses using a Ricker's P wavelet. Top figures show the horizontal component and bottom figures show the vertical component: (a) wavelet with 5 s period and 30° incidence; (b) wavelet with 3 s period and 75° incidence

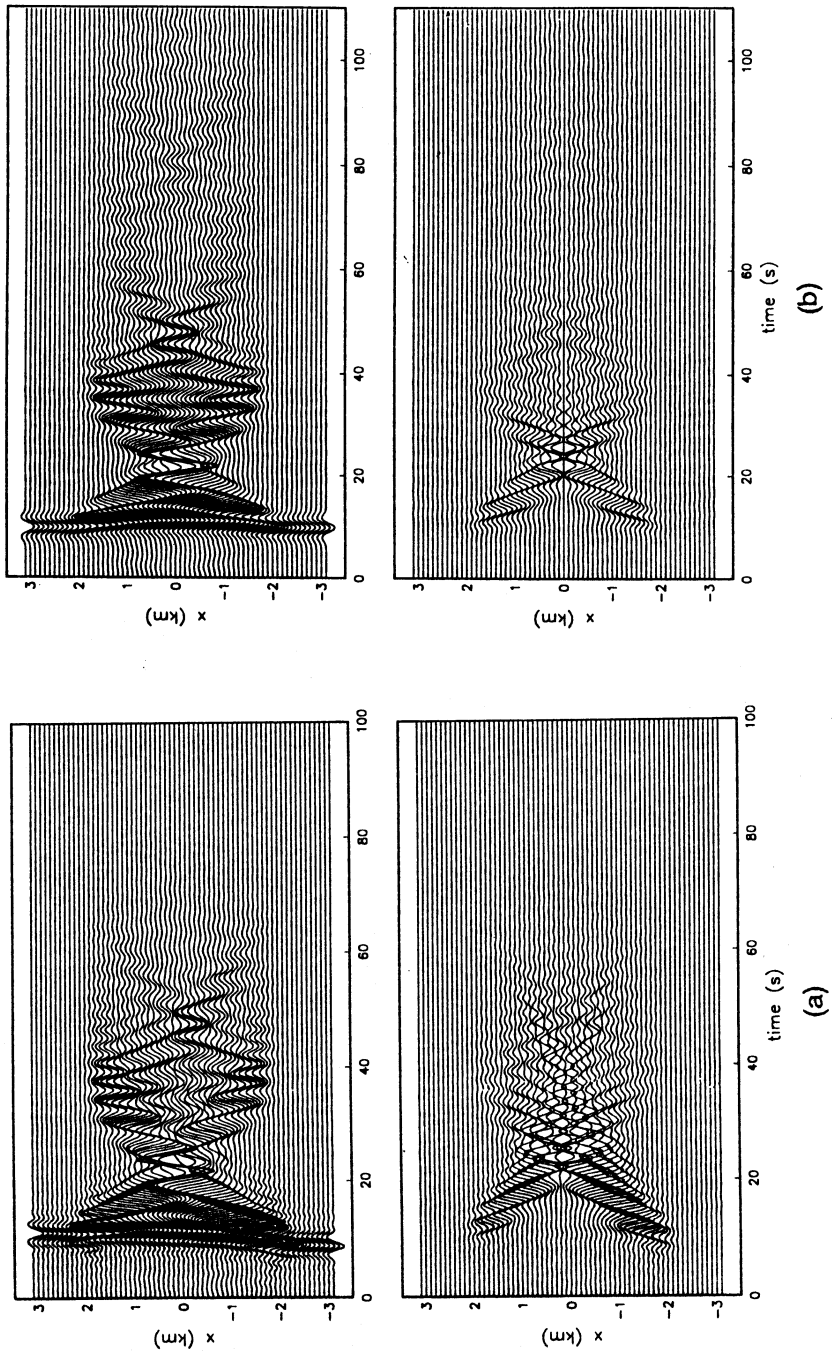

Figure 15. Time–responses using a Ricker's SV-wavelet. Top figures show the horizontal component and bottom figures show the vertical component: (a) wavelet with 3 s period and 30° incidence; (b) wavelet with 5 s period and vertical incidence

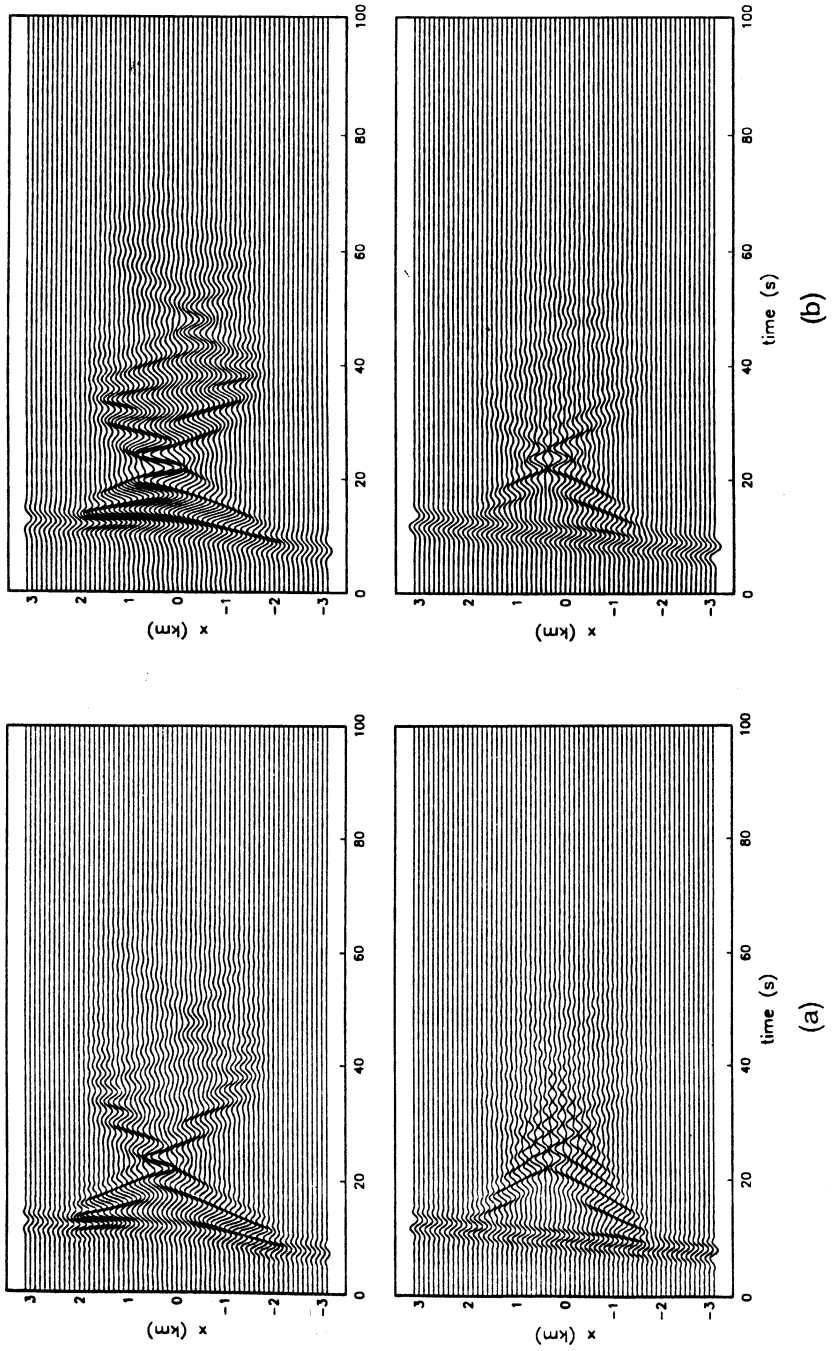

Figure 16. Time–responses using a Ricker's Rayleigh wavelet. Top figures show the horizontal component and bottom figures show the vertical component: (a) wavelet with 3 s; (b) wavelet with 5 s

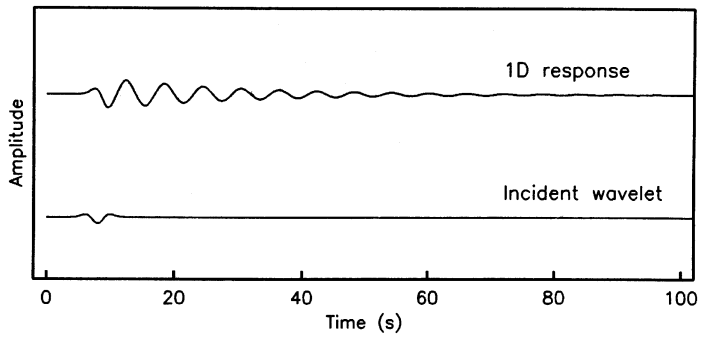

Figure 17. One-dimensional time–response of a vertically incident S-wavelet for the corresponding TB site ($H = 145$ m)

CONCLUSIONS

A direct boundary element method formulated with isoparametric quadratic boundary elements, for calculating the 2D scattering of seismic waves due to incident P-, SV- and Rayleigh waves was briefly presented.

A comparison between 1D results and the observed amplification at site 84 located at the zone of heavy damage during the 1985 earthquake was presented. It was shown that the 1D theory, on average, can explain most of the observed amplification at site 84. This conclusion is valid for all zones where structural damage has been observed during recent earthquakes.

Data recorded at site TB, located at the centre of a thick alluvial deposit, were used to probe that irregular amplification effects have been observed there: this site could possibly has been affected by 3D effects due to different azimuth of incoming earthquakes. The 2D method presented here was used to model a NS section of the valley where site TB is located. The 1989 earthquake was chosen because it was assumed that the incoming azimuth did not produce 3D effects. Results with the proposed 2D geometry are closer to the observations than the 1D results suggesting, at least qualitatively, that site TB could have been affected by 2D and 3D effects. The amplification pattern both in frequency and time domains observed for P-, SV- and Rayleigh waves was fairly similar, showing that probably the same mechanism of amplification is presented for all waves.

ACKNOWLEDGEMENTS

This research was supported by the National Council for Science and Technology (*CONACyT*) and by the Government of Mexico City (*Secretaría General de Obras y Servicios del Departamento del Distrito Federal*). The modelling part of this work was developed at the Wessex Institute of Technology, UK, while the processing of the accelerometric data are due to research at the *Centro de Investigación Sísmica*, Mexico. Accelerometric data presented here was collected by the *Instituto de Ingeniería*, *UNAM*, and by the *Centro de Instrumentación y Registro Sísmico*. The critical review of this paper by Mario Ordaz, Francisco Sánchez-Sesma and one anonymous reviewer is greatly appreciated.

REFERENCES

1. J. E. Vidale and D. V. Helmberger, 'Elastic finite-difference modeling of the 1971 San Fernando, California earthquake', *Bull. seismol. soc. Am.* **78**, 122–141 (1988).
2. N. Moeen-Vaziri and M. D. Trifunac, 'Scattering and diffraction of plane *P* and *SV* waves by two-dimensional inhomogeneities: Part II', *Soil dyn. earthquake eng.* **7**, 189–200 (1988).

3. D. Jongmans and M. Campillo, 'The response of the Ubaye valley (France) for incident *SH* and *SV* waves: comparison between measurements and modeling', *Bull. seism. soc. Am.* **83**, 907–924 (1993).
4. A. S. Papageorgiou and J. Kim, 'Propagation and amplification of seismic waves in 2D valleys excited by obliquely incident P- and SV-waves', *Int. j. earthquake eng. struct. dyn.* **22**, 167–182 (1993).
5. P.-Y. Bard, M. Campillo, F. J. Chávez-García and F. J. Sánchez-Sesma, 'The Mexico earthquake of september 19, 1985 — a theorethical investigation of large- and small-scale amplification effects in the Mexico City Valley', *Earthquake spectra* **4**, 609–633 (1988).
6. M. Campillo, P.-Y. Bard, F. Nicollin and F. J. Sánchez-Sesma, 'The Mexico earthquake of september 19, 1985 – the incident wave field in Mexico City during the great Michoacan earthquake and its interaction with the deep basin', *Earthquake spectra* **4**, 591–608 (1988).
7. F. J. Sánchez-Sesma, F. J. Chávez-García and M. A. Bravo, 'Seismic response of a class of alluvial valleys for incident *SH* waves', *Bull. seismol. soc. Am.* **78**, 83–95 (1988).
8. M. Campillo, F. J. Sánchez-Sesma and K. Aki, 'Influence of small lateral variations of a soft surficial layer on seismic ground motion', *Soil dyn. earthquake eng.* **9**, 284–288 (1990).
9. R. Paolucci and E. Faccioli, 'Analysis of spatial variation of earthquake ground motion in the Mexico City area', *Proc. 4th int. conf. of seismic zonation*, Stanford, CA, Vol. 2, 1991, pp. 319–326.
10. P. K. Hadley, A. Askar and A. S. Cakmak, 'Subsoil geology and soil amplification in Mexico Valley', *Soil dyn. earthquake eng.* **10**, 101–110 (1991).
11. L. E. Pérez-Rocha, F. J. Sánchez-Sesma and E. Reinoso, 'Three- dimensional site effects in Mexico City: evidences from accelerometric network observations and theoretical results', *Proc. 4th int. conf. of microzonation*, Vol. 2, 1991, pp. 327–334.
12. F. J. Sánchez-Sesma, L. E. Pérez-Rocha and E. Reinoso, 'Ground motion in Mexico City during the April 25, 1989, Guerrero earthquake', *Tectonophysics* **218**, 127–140 (1993).
13. H. Kawase and K. Aki, 'A study of the response of a soft basin for incident *S*, *P*, and Rayleigh waves with special reference to the long duration observed in Mexico City', *Bull. seismol. soc. Am.* **79**, 1361–1382 (1989).
14. S. K. Singh and M. Ordaz, 'On the origin of the long coda observed in the lake-bed strong-motion records of Mexico City', *Bull. seismol. soc. Am.* **83**, 1298–1306 (1993).
15. F. J. Chávez-García and P.-Y. Bard, 'Site effects in Mexico City eight years after the September 1985 Michoacan earthquakes', *Soil dyn. earthquake eng.* **13**, 229–247 (1994).
16. M. Ordaz and E. Faccioli, 'Site response analysis in the Valley of Mexico: selection of input motion and extent of non-linear soil behaviour', *Int. j. earthquake eng. struct. dyn.* **23**, 895–908 (1994).
17. D. Fäh, P. Suhadolc, St. Mueller and G. P. Panza, 'A hybrid method for the estimation of ground motion in the sedimentary basins: quantitative modelling for Mexico City', *Bull. seismol. soc. Am.* **84**, 383–399 (1994).
18. J. Domínguez, *Boundary Elements in Dynamics*, Comp. Mech. Publications, Southampton, U.K., 1993.
19. H. L. Wong, 'Effect of surface topography on the diffraction of *P*, *SV*, and Rayleigh waves', *Bull. seismol. soc. Am.* **72**, 1167–1183 (1982).
20. M. Dravinski and T. S. Mossessian, 'Scattering of plane harmonic *P*, *SV*, and Rayleigh waves by dipping layers of arbitrary shape', *Bull. seismol. soc. Am.* **77**, 212–235 (1987).
21. H. Kawase, 'Irregular ground analysis to interpret time-characteristics of strong ground motion recorded in Mexico City during 1985 Mexico earthquake', in *Ground Motion and Engineering Seismology*, Ed. A. S. Cakmak, *Development in Geotechnical Engineering*, Vol. 44, Elsevier, Amsterdam, (1987), pp. 467–476.
22. H. Kawase, 'Time–domain response of a semi-circular canyon for incident *SV*, *P*, and Rayleigh waves calculated by the discrete wavenumber boundary element method', *Bull. seismol. soc. Am.* **78**, 1415–1437 (1988).
23. F. J. Sánchez-Sesma and M. Campillo, 'Diffraction of *P*', *SV*, and Rayleigh waves by topographic features: a boundary integral formulation', *Bull. seismol. soc. Am.* **81**, 2234–2253 (1991).
24. E. Reinoso, 'Seismic effects in the valley of Mexico: measured amplification at lake-bed zone sites', *Proc. 9th nat. conf. of earthquake engineering*, Manzanillo, Mexico, Vol. 1, 1991, pp. 63–76.
25. E. Reinoso, L. C. Wrobel and H. Power, 'Preliminary results of the modelling of the Mexico City Valley with a two-dimensional boundary element method for the scattering of *SH* waves', *Soil dyn. earthquake eng.* **12**, 457–468 (1993).
26. E. Reinoso, 'Boundary element modelling of scattering from topographical structures with applications to the Mexico City Valley', Ph.D. Thesis, Wessex Institute of Technology, University of Portsmouth, Southampton, U.K., 1994.
27. S. K. Singh, J. Lermo, T. Domínguez, M. Ordaz, J. M. Espinosa, E. Mena and R. Quaas, 'A study of amplification of seismic waves in the Valley of Mexico with respect to a hill zone site', *Earthquake spectra* **4**, 653–673 (1988).
28. S. K. Singh, R. Quaas, M. Ordaz, F. Mooser, D. Almora, M. Torres and R. Váquez, 'Is there truly a "hard" rock site in the Valley of Mexico?', *Geophys. res. lett.* **22**, 482–484 (1995).
29. E. Rosenblueth, F. J. Sánchez-Sesma, M. Ordaz and S. K. Singh, 'Design spectra for Mexico's Federal District', *Earthquake spectra* **5**, 273–292 (1988).
30. M. P. Romo and H. B. Seed, 'Analytical modeling of dynamic soil response in the Mexico earthquake of September 19, 1985', in M. A. Cassaro and E. M. Romero (eds) *Mexico Earthquakes — 1985*, Am. Soc. Civil Engineers, 1986.

31. H. B. Seed, M. P. Romo, J. I. Sun, A. Jaime and J. Lysmer, 'Relationships between soil conditions and earthquake ground motion', *Earthquake spectra* **4**, 687–729 (1988).
32. M. Ordaz, M. A. Santoyo, S. K. Singh and R. Quass, 'Analysis of the bore-hole recordings obtained in Mexico City during the May 31, 1990 earthquake', *Proc. int. symp. the effects of surf. geol. on seis. motion*, ESG1992, Odawara, Japan, Vol. 1, 1992, pp. 155–160.
33. J. Iglesias, 'Seismic zoning of Mexico City after the 1985 earthquake', *Earthquake spectra* **5**, 257–272 (1988).

